ACCURATE TERAHERTZ IMAGING SIMULATION WITH RAY TRACING INCORPORATING BEAM SHAPE AND REFRACTION

Pavel Paramonov, Lars-Paul Lumbeeck, Jan De Beenhouwer, Jan Sijbers

imec-VisionLab, Department of Physics, University of Antwerp, Antwerp, Belgium

ABSTRACT

In this paper, we present an approach to realistically simulate terahertz (THz) transmission mode imaging. We model the THz beam shape and account for the refraction of the THz beam at the different media interfaces using ray optics. Our approach does not require prior knowledge on the interfaces, instead it utilizes the refractive index scalar field. We study the beam shape and refraction effects separately by comparing resulting sinograms with the ones simulated by a Gaussian beam model, as well as with a real acquisition of a plastic object. The proposed forward projection can be utilized in iterative reconstruction algorithms to improve the quality of THz CT images.

***Index Terms*—** Terahertz imaging, computed tomography, ray tracing, terahertz beam, forward projection

1. INTRODUCTION

The frequencies of THz waves range from 0.1 to 10 THz, and the corresponding wavelengths from 3 mm to 30 μm [1]. THz CT application domains range from detecting hidden organic materials [2] and examining artwork [3], to detecting hidden objects for security purposes (textiles are transparent for THz waves) [4]. Studying the objects internal structure [5] and quality inspection [6] are the examples of an industrial application of THz CT. The low energy of THz radiation and its non-ionizing property make it attractive for the medical domain (e.g. skin scanning in reflection mode for cancer diagnostics [7, 8]).

In recent years, powerful reconstruction toolboxes were developed for the X-Ray CT. One of them is the ASTRA toolbox, which combines great flexibility in projection geometry with an efficient GPU implementation of various reconstruction algorithms [9]. Although many advanced CT reconstruction methods have been developed in the field of X-ray CT, they cannot be directly applied to THz CT. The two main reasons are the finite Gaussian beam profile of the THz radiation and beam refraction at material interfaces. The first results in projection blur, while the second results in abrupt drops of detected intensity near the interfaces.

Various applications of THz radiation require different imaging setup. In diffraction tomography the scattering potential distribution of an object is reconstructed based on the detected diffracted THz wave. There, THz radiation is described by either Born or Rytov approximation of the wave equation [10, 11, 12]. Alternatively, the beam can be focused on an object, followed by a point-by-point scan in either transmission or reflection mode. The latter one is preferred when transmission measurement is impossible, e.g., due to high water absorption [12, 13]. Examples of transmission mode THz scanning simulation can be found in [5, 14, 15], where THz radiation is simulated with ray tracing technique. In [5, 15] beam is approximated with a finite number of rays, when each ray can be refracted and reflected independently from the others.

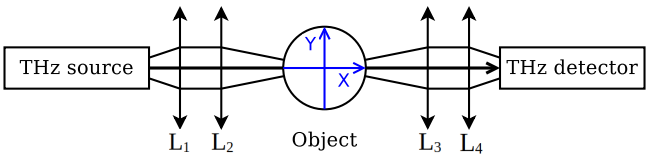

Fig. 1. Typical transmission mode THz imaging setup.

In this paper, we present a 2D forward projection model of transmission mode imaging that takes both the beam shape and refraction into account without prior knowledge of material interfaces. The model is based on ray tracing, which is widely used for the simulation of light propagation. We validated our model on simulated data and compared the resulting sinogram to a real acquisition of a plastic object.

2. THZ IMAGING SIMULATION

In order to simulate transmission mode THz forward projection, we consider three major features of THz imaging setup: raster scanning acquisition projection geometry, beam shape, and beam refraction at the interfaces. We describe each of them separately in the following subsections.

2.1. Projection geometry

A typical transmission mode THz imaging system includes collimating lenses L_1, L_3, and focusing lenses L_2, L_4 (see Fig. 1) [1, 15, 16]. In this 2D schematic, the beam is propagating along the x-axis, and the object is placed on a rotation

stage, which is attached to the translation stage to perform pixel-wise scanning. To achieve the best possible resolution, the sample needs to be fixed in the focal point, which is assumed to be the center of coordinates. This procedure is then repeated for every projection angle θ.

The imaging setup from Fig. 1 resembles the parallel beam geometry of raster-based X-ray scanning. Here however, due to the beam shape with non-zero waist and beam refraction, the size of lens L_3, the distance from source to sample, as well as from the sample to the detector all play an important role in how much intensity will be detected on a pixel. Thus we update the parallel beam geometry with the mentioned parameters (see Fig. 2, where SO is the distance from the source to the center of coordinates, and OD is the distance from the center of coordinates to the detector).

To simulate the THz beam, we cast multiple rays and compute the ray intensity at the end of its path L according to the Beer-Lambert law:

$$R_\theta^j(t) = R_0 e^{-\int_L \mu(x,y)ds}, \quad j = 1, \ldots, N_R, \tag{1}$$

where R_0 is the initial ray intensity, $\mu(x, y)$ is the attenuation coefficient at (x, y), and N_R is the number of rays cast per beam. When all the rays are traced up to the end of the volume, the resulting detected intensity value is stored in the detector pixel:

$$d_\theta(t) = \frac{N_d}{N_R} \sum_{j=1}^{N_R} R_\theta^j(t), \tag{2}$$

where N_d is the number of rays that hit the detector.

This approach allows not only to take the THz beam shape into account, but also refraction.

2.2. THz beam model

The THz beam intensity can be approximated with a Gaussian function [17]. The beam intensity $I(x, y, z)$ at a location (x, y, z) of the 3D beam with wavelength λ and waist w_0 propagating through the air along the z dimension is defined as follows:

$$I(x, y, z) = I_0 \left(\frac{w_0}{w(z)} \right)^2 \exp\left(-\frac{2\left(x^2 + y^2\right)}{w^2(z)} \right), \tag{3}$$

where $w(z) = w_0 \sqrt{1 + \left(\frac{z}{z_r}\right)^2}$ is the beam radius, and $z_r = \frac{\pi w_0^2}{\lambda}$ is the Rayleigh range.

In this paper, we use 2D Gaussian beam propagating along the x-axis [18]:

$$I(x, y) = I_0 \sqrt{\frac{\pi}{2}} \frac{w_0^2}{w(x)} \exp\left(-\frac{2y^2}{w^2(x)} \right). \tag{4}$$

To simulate the 2D THz beam, we follow the approach proposed in [15]. It is based on casting multiple rays towards the beam focal point, where each ray is defined by a randomly sampled offset along the beam slice axis $\psi \sim \mathcal{N}\left(0, \sigma_\psi^2\right)$ and its angle with propagation axis $\phi \sim \mathcal{N}\left(0, \sigma_\phi^2\right)$. We will refer to this model as Monte Carlo based Ray Tracing (MC-RT).

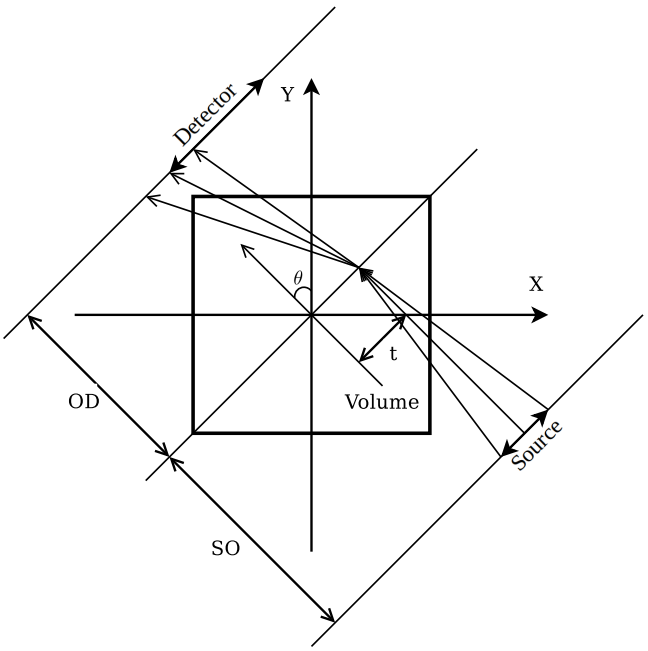

Fig. 2. Forward projection geometry for THz CT.

2.3. Beam refraction

We account for refraction in the forward projection as it has been shown to increase reconstruction quality [14]. Refraction is usually computed on known interfaces [5, 14], however, prior information on the interfaces (e.g., from the CAD model) is not always available. Yet it is possible to provide at least the first guess of the refractive index scalar field and use it for ray direction updates during ray tracing. Then, the refractive index map can be updated during an iterative reconstruction. This approach is commonly applied to create realistic volume render (e.g., in [19, 20]). One way to utilize the refractive index scalar field is based on the differential equation that describes ray propagation through the continuous scalar field $\eta(x, y)$ that defines refractive index at (x, y) [19]:

$$\frac{d}{ds}\left(\eta \frac{d\vec{r}}{ds}\right) = \vec{\nabla}\eta, \tag{5}$$

where $\vec{r}$ is the ray direction. Eq. (5) requires $\eta(x, y)$ to be differentiable, which in turn requires a smooth function. On the other hand, oversmoothing of $\eta(x, y)$ leads to a "slower" change of $\vec{r}$, which results in significant displacement of the refraction point. This can be a problem when simulating refraction on objects with sharp edges and high refractive index

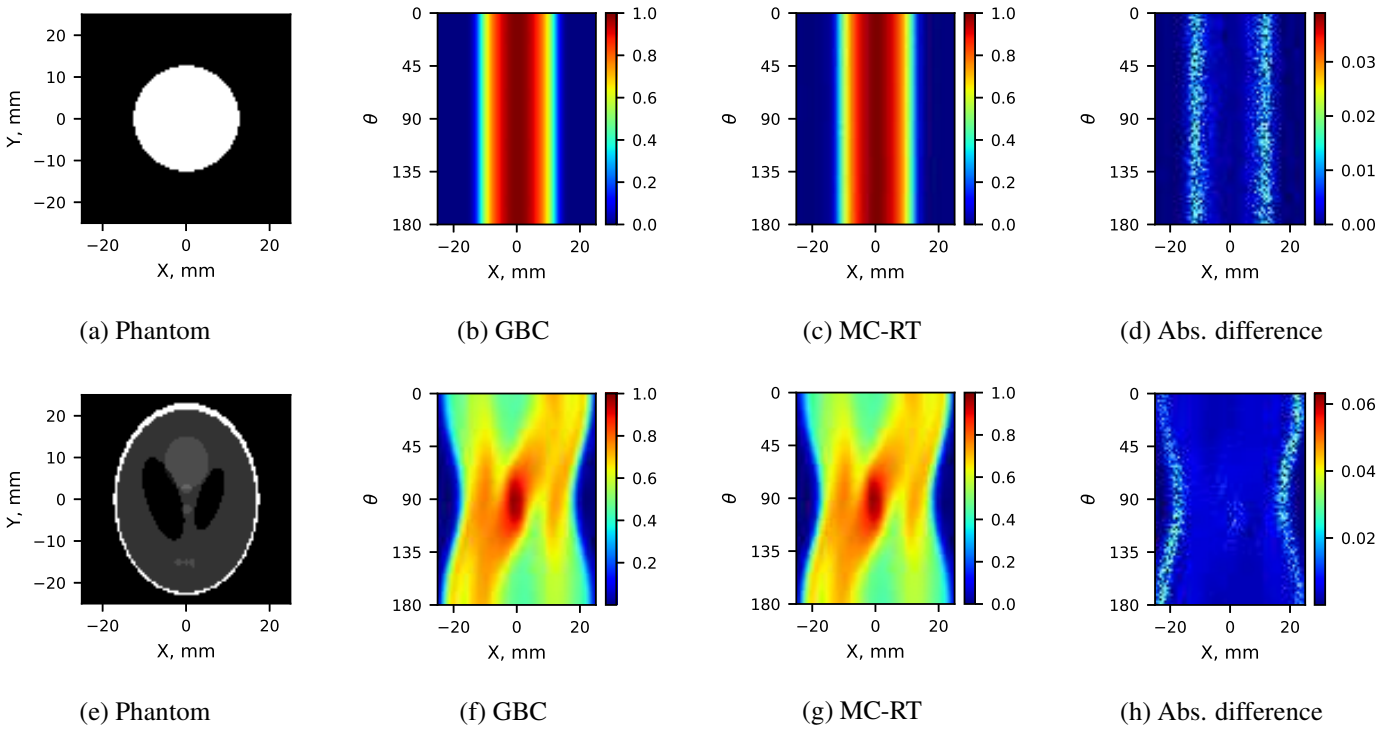

Fig. 3. Beam shape artifact in simulated sinograms. Gaussian beam is simulated with $\lambda = 1mm$, $w_0 = 3mm$, MC-RT is run with 10^3 rays per beam.

(e.g., plastic objects). In our work, we implemented refraction at the pixel edge, where unit vector $\frac{\vec{\nabla}\eta}{|\vec{\nabla}\eta|}$ is used as a surface normal vector, as proposed in [21]. This approach leads to a smaller displacement of the refraction point than ray tracing based on Eq. (5).

3. EXPERIMENTS AND RESULTS

Simulation experiments were set up to validate the proposed THz forward projection simulator.

3.1. Beam shape evaluation

We evaluate the beam shape simulation by comparing the resulting sinogram with the one simulated using the 2D Gaussian from Eq. (4), where each projection pixel $p_\theta(t)$ is computed as

$$p_\theta(t) = \int_{-\infty}^{\infty}\int_{-\infty}^{\infty} g(x,y)\delta(x\cos\theta + y\sin\theta - t)dxdy, \quad (6)$$

where $g(x,y) = f(x,y) * I_\theta(x,y)$, and $I_\theta(x,y)$ is the 2D Gaussian beam intensity at angle θ. We further refer to this model as Gaussian Beam Convolution (GBC). Each pixel of the GBC sinogram is a measure of the beam attenuation, while our forward projection simulation returns the intensity value for the detector pixel. To compare the two sinograms, we compute the log transform of the MC-RT sinogram: $\hat{p}_\theta(t) = -\log\left(\frac{d_\theta(t)}{d_0}\right)$, where d_0 is the detected intensity without an object, then normalize both sinograms with their maximal values (see Fig. 3). The more rays are cast for MC-RT, the better the Gaussian beam is approximated (see Fig. 4). On the other hand, this makes MC-RT more time consuming (e.g., for a 400×400 Shepp-Logan phantom MC-RT takes ~ 500 sec. on an Intel Core i7-9700K CPU).

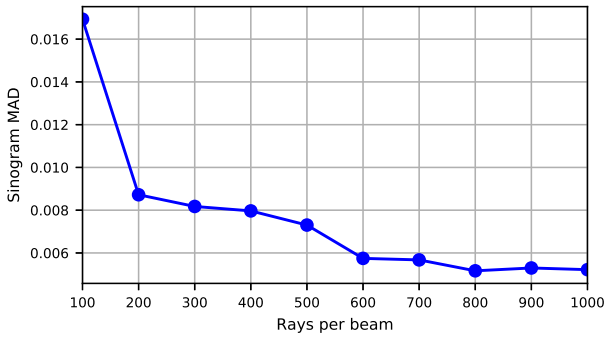

Fig. 4. Mean absolute difference (MAD) between GBC and MC-RT sinograms for the Shepp-Logan phantom.

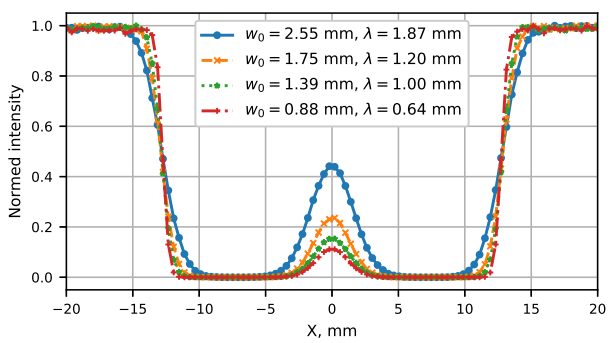

Fig. 5. Simulation of acquisition of a cylinder object. MC-RT is run with 10^5 rays per beam, the refractive index of the sample is set to 1.77.

3.2. Refraction evaluation

To validate our forward projection, we simulate the acquisition of the cylinder made of PEEK originally described in [16]. The cylinder diameter is 25 mm and refractive index is 1.77 (see Fig. 5). Refraction can direct the beam away from the detector, possibly resulting in projection regions with zero detected intensity, as is clearly visible in the projection of the cylinder sample. The decrease in intensity depends on the wavelength and the beam waist, as well as the transmission coefficient. A qualitative comparison shows good agreement to the measured data obtained in Fig. 10a of [16].

4. CONCLUSION AND FUTURE WORK

The proposed approach is able to realistically simulate THz imaging by taking into account the THz beam shape and the THz beam refraction. Experiments showed that MC-RT is equivalent to the GBC model, but unlike the latter MC-RT allows to take refraction into account. On the other hand, MC-RT quickly becomes time consuming with increasing number of traced rays. As future work, we intend to incorporate our simulation in iterative reconstruction algorithms as a forward projection model, as well as to extend it to 3D.

5. ACKNOWLEDGMENTS

We wish to thank Lei Zhang of imec USA-Florida for fruitful discussions on THz imaging setups, and Marina Ljubenovic for discussions on the THz beam shape effects.

6. REFERENCES

[1] W.L. Chan, J. Deibel, and D.M. Mittleman, "Imaging with terahertz radiation," *Reports on Progress in Physics*, vol. 70, pp. 1325–1379, August 2007.

[2] M. Bessou, H. Duday, J.-P. Caumes, S. Salort, B. Chassagne, A. Dautant, A. Ziéglé, and E. Abraham, "Advantage of terahertz radiation versus X-ray to detect hidden organic materials in sealed vessels," *Optics Communications*, vol. 285, pp. 4175–4179, October 2012.

[3] J.B. Jackson, J. Bowen, G. Walker, J. Labaune, G. Mourou, M. Menu, and K. Fukunaga, "A survey of terahertz applications in cultural heritage conservation science," *IEEE Transactions on Terahertz Science and Technology*, vol. 1, pp. 220–231, September 2011.

[4] M. Kowalski, "Hidden object detection and recognition in passive terahertz and mid-wavelength infrared," *Journal of Infrared, Millimeter, and Terahertz Waves*, vol. 40, pp. 1074–1091, December 2019.

[5] S. Mukherjee, J. Federici, P. Lopes, and M. Cabral, "Elimination of fresnel reflection boundary effects and beam steering in pulsed terahertz computed tomography," *Journal of Infrared, Millimeter, and Terahertz Waves*, vol. 34, pp. 539–555, September 2013.

[6] F. Ellrich, M. Bauer, N. Schreiner, A. Keil, T. Pfeiffer, J. Klier, S. Weber, J. Jonuscheit, F. Friederich, and D. Molter, "Terahertz quality inspection for automotive and aviation industries," *Journal of Infrared, Millimeter, and Terahertz Waves*, vol. 41, pp. 470–489, April 2020.

[7] E. Pickwell and V. P. Wallace, "Biomedical applications of terahertz technology," *Journal of Physics D: Applied Physics*, vol. 39, pp. R301–R310, September 2006.

[8] R.M. Woodward, B.E. Cole, V.P. Wallace, R.J. Pye, D.D. Arnone, E.H. Linfield, and M. Pepper, "Terahertz pulse imaging in reflection geometry of human skin cancer and skin tissue," *Physics in Medicine and Biology*, vol. 47, pp. 3853–3863, November 2002.

[9] W. Van Aarle, W.J. Palenstijn, J. Cant, E. Janssens, F. Bleichrodt, A. Dabravolski, J. De Beenhouwer, K. J. Batenburg, and J. Sijbers, "Fast and flexible X-ray tomography using the ASTRA toolbox," *Optics Express*, vol. 24, pp. 25129–25147, October 2016.

[10] S. Wang, B. Ferguson, D. Abbott, and X.-C. Zhang, "T-ray imaging and tomography," *Journal of Biological Physics*, vol. 29, pp. 247–256, June 2003.

[11] S. Wang and X.-C. Zhang, "Pulsed terahertz tomography," *Journal of Physics D: Applied Physics*, vol. 37, pp. R1–R36, February 2004.

[12] J.P. Guillet, B. Recur, L. Frederique, B. Bousquet, L. Canioni, I. Manek-Hönninger, P. Desbarats, and P. Mounaix, "Review of terahertz tomography techniques," *Journal of Infrared, Millimeter, and Terahertz Waves*, vol. 35, pp. 382–411, April 2014.

[13] H. Guerboukha, K. Nallappan, and M. Skorobogatiy, "Toward real-time terahertz imaging," *Advances in Optics and Photonics*, vol. 10, pp. 843–938, December 2018.

[14] J. Tepe, T. Schuster, and B. Littau, "A modified algebraic reconstruction technique taking refraction into account with an application in terahertz tomography," *Inverse Problems in Science and Engineering*, vol. 25, pp. 1448–1473, October 2017.

[15] A. Duhant, M. Triki, and O. Strauss, "Terahertz differential computed tomography: a relevant nondestructive inspection application," *Journal of Infrared, Millimeter, and Terahertz Waves*, vol. 40, pp. 178–199, February 2019.

[16] A. Brahm, A. Wilms, M. Tymoshchuk, C. Grossmann, and G.Notni A. Tünnermann, "Optical effects at projection measurements for terahertz tomography," *Optics and Laser Technology*, vol. 62, pp. 49–57, October 2014.

[17] B. Recur, J.P. Guillet, I. Manek-Hönninger, J.C. Delagnes, W. Benharbone, P. Desbarats, J.P. Domenger, L. Canioni, and P. Mounaix, "Propagation beam consideration for 3D THz computed tomography," *Optics Express*, vol. 20, pp. 5817–5829, March 2012.

[18] L.-P. Lumbeeck, P. Paramonov, J. Sijbers, and J. De Beenhouwer, "The radon transform for terahertz computed tomography incorporating the beam shape," in *Proceedings - International Conference on Image Processing, ICIP 2020*. In press.

[19] J.G. Magnus and S. Bruckner, "Interactive dynamic volume illumination with refraction and caustics," *IEEE Transactions on Visualization and Computer Graphics*, vol. 24, pp. 984–993, January 2018.

[20] I. Ihrke, G. Ziegler, A. Tevs, C. Theobalt, M. Magnor, and H.P. Seidel, "Eikonal rendering: Efficient light transport in refractive objects," *ACM Transactions on Graphics*, vol. 26, July 2007.

[21] M. Hadwiger, C. Sigg, H. Scharsach, K. Bühler, and M. Gross, "Real-time ray-casting and advanced shading of discrete isosurfaces," *Computer Graphics Forum*, vol. 24, pp. 303–312, September 2005.